Wetting of Fiber Mats for Composites Manufacturing: II. Air Entrapment Model

Yung-Tin Chen, Christopher W. Macosko, and H. Ted Davis
Dept. of Chemical Engineering and Materials Science, Center of Interfacial Engineering, University of Minnesota, Minneapolis, MN 55455

In this work the experimental observations are explained with the aid of a simple air-entrapment model based on the concept of two levels of porosity of fiber mats. A simple model that includes liquid bypassing with initial air trapping, subsequent capillary invasion of regular fiber bundles with air compression, and finally mobilization is proposed to explain air-entrapment phenomena. The simple model successfully rationalizes the observed air trapping and compression during initial liquid–fiber contact. An empirical equation for the mobilization efficiency is adapted to the model to estimate void content. The velocity dependence of the trapped void content predicted by the model is in good agreement with observations.

Introduction

In Part I, we used a refractive index matching technique to visualize fiber wetting with a high-magnification video camera and a video-enhanced microscope. In this article, we explain our experimental observations with the aid of a simple air-entrapment model, which includes liquid bypassing with initial air trapping, subsequent capillary invasion of regular fiber bundles with air compression, and mobilization. The purpose is to explain qualitatively the flow phenomena observed in our wetting visualization experiments. For a quantitative comparison, a more realistic working model for void content prediction, one that includes capillary invasion of disordered fiber bundles, must be developed. However, an engineering approach to estimate void content based on the current simple models is proposed and described at the end of this work.

Theoretical Background

In order to understand the fiber-wetting process, it is important to realize that in commercially used fiber mats there are two levels of permeabilities. These are the permeability of the "tight' pore space inside the fiber bundles and that of the larger pore space around fiber bundles. The two levels of impregnation flow will be described as Darcy's flow through fiber mats, and microscopic flow penetrating into fiber tows or bundles. The pore sizes around fiber bundles can be larger than that inside fiber bundles by orders of magnitude. This results in much less permeability inside the fiber bundles. The macroscopic main flow can be described conventionally with Darcy's law:

$$\phi_m V_x = \frac{K_m}{\eta}\frac{\Delta P}{\Delta x}, \tag{1}$$

where ϕ_m is the mat porosity, η is the fluid viscosity, V_x is the superficial velocity, and ΔP is the pressure difference between Δx. The mat permeability, K_m, can be estimated from Kozeny's equation:

$$K_m = \frac{D_p^2 \phi^3}{C_K (1-\phi)^2}, \tag{2}$$

where D_p is the diameter of the fiber bundle, ϕ is the porosity, and C_k is an empirical constant. The value of C_k ranges from 150 to 200 for spherical particles. For fibrous mats the C_k value was experimentally determined as about 180 (Gonzalez, 1983; Chen, 1993). A detailed discussion of Kozeny's constant can be found in Skartsis et al. (1992a). The permeabilities of the fiber mats can be hundreds of times greater than those of fiber bundles because of the large differences of porosities.

The flow inside fiber bundles is mostly controlled by capillary action, thus the surface interaction between fiber and resin must be designed to give good wetting properties. The

capillary action inside fiber bundles can be expressed as (Van Brakel and Heertjes, 1977; Gonzalez, 1983; Macosko, 1989):

$$L_p^2 = \left(\frac{2K_b}{\phi_b \eta}\right)\left(\frac{2\sigma \cos\theta}{r}\right)t, \tag{3}$$

where L_p is the penetration length, K_b is the fiber bundle permeability, ϕ_b is the fiber bundle porosity, σ is the surface tension, θ is the wetting angle, η is the viscosity, t is the time, and r is the radius of average pore size between fibers. The ratio of macroscopic main velocity, V_x, and capillary velocity, V_{cap}, can be defined as

$$V^* = \frac{V_x}{V_{cap}} = \left(\frac{K_m \phi_b}{K_b \phi_m}\right)\left(\frac{r\Delta P}{2\sigma \cos\theta}\right). \tag{4}$$

This dimensionless velocity is an important factor in understanding air entrapment.

Simple Air Entrapment Models

Model of liquid bypassing and initial air trapping for transverse flow

We first examine the liquid bypassing and initial air trapping for transverse flow. Consider two cylindrical fiber bundles separated by a distance d. Most of the invading liquid will bypass through the passage between the two fiber bundles (Figure 1). During bypassing, the liquid will penetrate into the fiber bundles owing to capillary suction and the external pressure. The amount of air entrapped when the liquid passes over the fiber bundles depends on how fast the invading speed is and how strong the capillary action is.

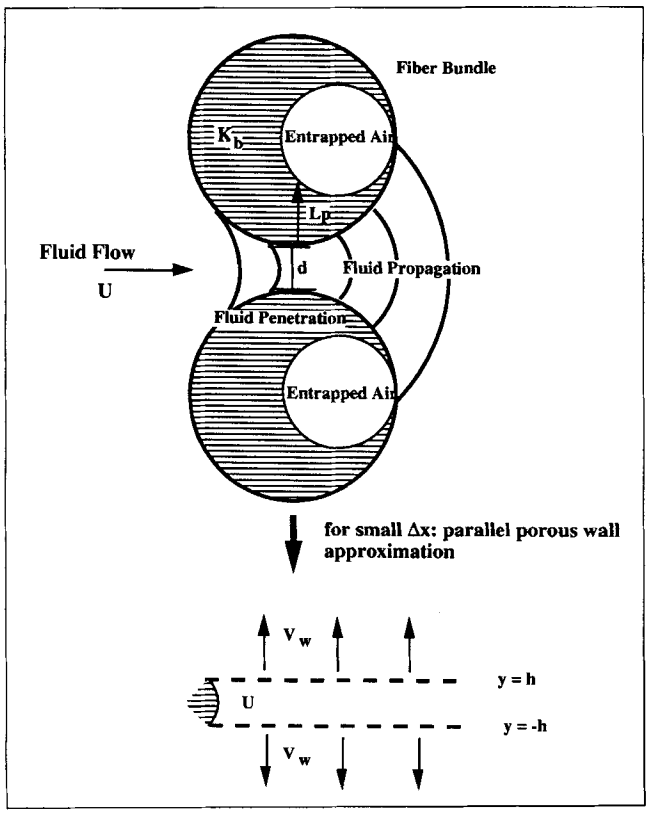

Figure 1. Initial air trapping model.
Parallel porous wall approximation applied.

This process can be simulated as a liquid penetrating a porous material, the porous material being a cylindrical fiber bundle. For a low porosity system, we assume that the flow field between the fiber bundles is unaffected by liquid penetration into the fiber bundles, but the overall mass balance along the external passage is preserved. For a small distance along the surface of the fibrous wall, the flow geometry can be simplified as flow across a flat porous wall. Thus, as an approximation, we can sum up all the small elements along the whole region and obtain the pressure distribution. That is, the converging–diverging throat shown in Figure 1 is divided into short segments and the flow in each segment is approximated as flow between parallel walls whose separation equals the average separation of the surfaces in that segment. The equations describing flow between parallel porous walls are summarized as follows (Berman, 1953):

Continuity (incompressible liquid):

$$\frac{\partial u}{\partial x} + \frac{1}{h}\frac{\partial v}{\partial \lambda} = 0; \qquad \lambda = y/h. \tag{5}$$

Momentum balance:

$$u\frac{\partial u}{\partial x} + \frac{v}{h}\frac{\partial u}{\partial \lambda} = -\frac{1}{\rho}\frac{\partial P}{\partial x} + \nu\left(\frac{\partial^2 u}{\partial x^2} + \frac{1}{h^2}\frac{\partial^2 u}{\partial \lambda^2}\right). \tag{6}$$

Boundary condition:

$$u(x, \pm 1) = 0; \qquad \frac{\partial u}{\partial \lambda}(x, 0) = 0 \tag{7}$$

$$v(x, \pm 1) = \pm v_w; \; v_w = \frac{K_b}{\eta \phi_b}\frac{\Delta P + \Delta P_{cap}}{L_p}, \tag{8}$$

where u and v are velocity components in the x and y direction, λ is a dimensionless variable in the y direction, h is the half gap thickness, ρ is the density, ν is the kinematic viscosity, ΔP is the pressure drop in the segment, ΔP_{cap} is the capillary pressure inside fiber bundle, and v_w is the porous wall velocity. The boundary condition is set to a constant wall velocity governed by Darcy's law. For a small segment length, Δx, this assumption is correct as long as the average external pressure difference, ΔP, and penetration length, L_p, are properly calculated. The approximate solutions of this parallel porous wall with constant wall velocity have been solved by Berman (1953) and White et al. (1958). For a small region from x_1 to x_2, the pressure drop is given by the equation

$$P(x_1) - P(x_2) = \frac{1}{2}\rho U_1^2\left(\frac{6\eta}{\rho h U_1} - \frac{162\, v_w}{35\, U_1}\right) \times \left(1 - \frac{v_w(x_2 - x_1)}{2U_1 h}\right)\left(\frac{x_2 - x_1}{h}\right), \tag{9}$$

where U_1 is the average inlet liquid velocity at x_1. Presum-

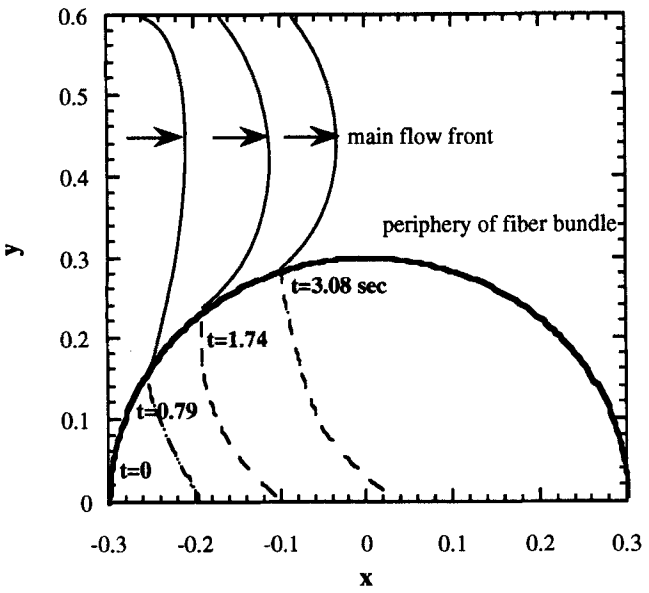

Figure 2. Simulated transient penetration length inside a fiber bundle at various instants.

Low flow velocity, 0.032 cm/s. No air entrapped in this flow rate. Material parameters are given in Table 1.

ably the microscopic flow takes place under creeping flow conditions.

With this solution, the relationship between time and the penetration length inside the fiber bundle can be readily found by taking into account the mass conservation law in the outside channels, namely,

$$U_2 h_2 = U_1 h_1 - \phi_b v_w \Delta x, \tag{10}$$

where U_1 and U_2 are the average velocity at position 1 and 2, h_1 and h_2 are the half gap thickness at position 1 and 2, and

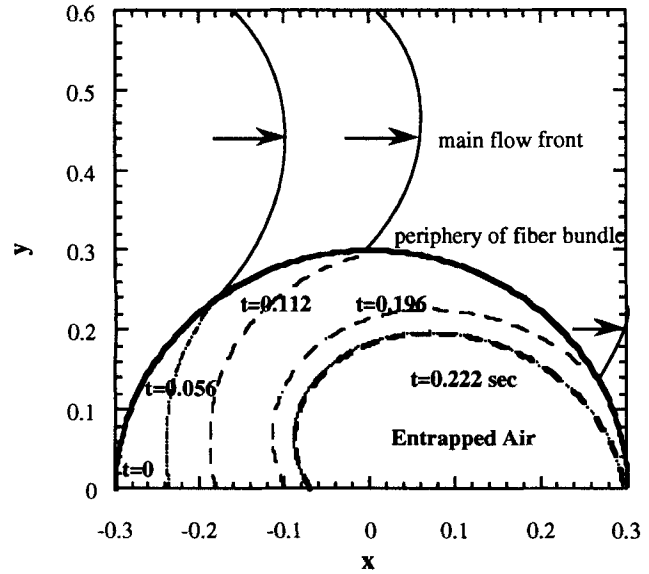

Figure 3. Same as Figure 2 but with high flow velocity, 1.13 cm/s.

Much air entrapped inside fiber bundle after the main flow passes by.

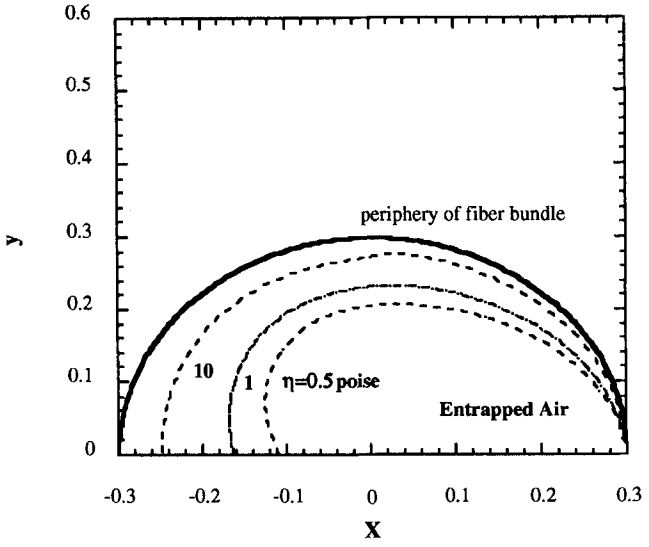

Figure 4. Effect of viscosity on initial entrapped void size.

Main flow velocity, 1.61 cm/s, surface tension, 50.5 dyne/cm. Viscosity is in poise.

ϕ_b is the porosity of a fiber bundle. As long as v_w is calculated from the current time step, the outlet velocity U_2 can be readily obtained from the preceding equation.

The liquid penetration inside fiber bundles can be obtained by a similar expression as Eq. 3. The driving force includes capillary pressure, ΔP_{cap}, and external pressure drop, ΔP, from the main flow. ΔP of each segment is time dependent and shall be updated at each time. The transient penetration lengths as a function of time for different initial velocities are illustrated in Figures 2 and 3. The parameters used in this work are listed in Table 1. The parameter values were determined experimentally. The details of how these parameters were obtained can be found in Chen (1993). The dashed curves of these figures are the invading liquid fronts. These curves are obtained by mapping the linear liquid penetration solutions to the cylindrical geometry by knowing the tangential angle and penetration length of each segment at a specific time. The main flow fronts corresponding to each instant of time are also sketched. At a slow liquid invading velocity (0.032 cm/s), there is no large air bubble entrapped inside the fiber bundle, while at a higher velocity (1.13 cm/s) large dry fiber areas are left behind the flow front (as indicated in Figure 3 at a time of 0.222 s). The amount of initial air entrapped increases with increasing viscosity. This is shown in Figure 4 with liquid viscosity of 0.5, 1 and 10 poise, respectively. With this model we are able to explain one of our major experimental results, namely, that the amount of

Table 1. Parameters Used in Model Prediction

Fibers	Oil
Fiber bundle radius = 0.3 cm	Viscosity = 51.5 cp
Interfiber spacing d = 0.02 cm	Surface tension = 50.5 dyne/cm
Fiber bundle porosity ϕ_b = 0.38	$\cos\theta$ = 0.45
Mat porosity ϕ_m = 0.7	
Bundle permeability $K_b = 3.56\times10^{-9}$ cm^{-2}	
Mat permeability $K_m = 2.5\times10^{-6}$ cm^{-2}	

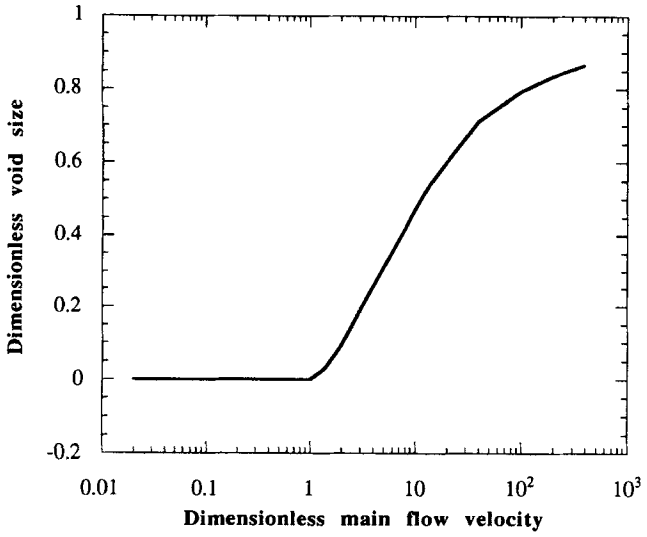

Figure 5. Initial dimensionless void size as a function of dimensionless velocity.

Dimensionless void size is the ratio of the area of entrapped air to that of fiber bundle. Dimensionless velocity is the ratio of measured liquid invading velocity to measured capillary velocity (Eq. 4).

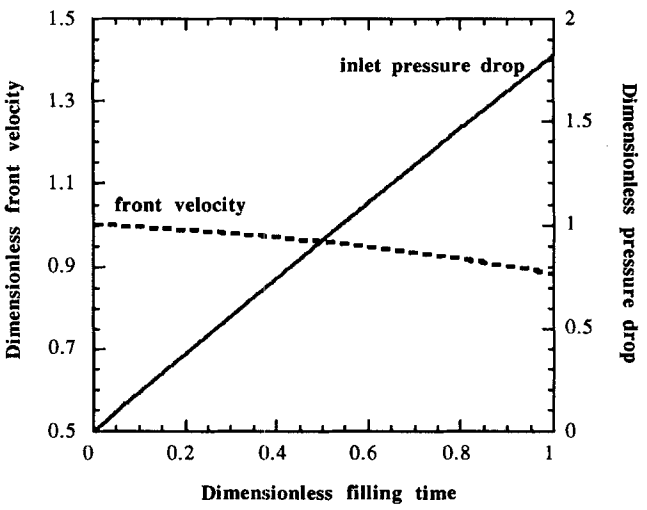

Figure 6. Evolution of front velocity and inlet pressure rise.

All parameters are scaled with respect to initial values or mold-filling time.

air entrapped inside fiber bundles increases with increasing velocity of the invading liquid.

Quantitative plots of calculated void size as a function of the dimensionless velocity are shown in Figure 5. Dimensionless void size is defined as the ratio of the area of entrapped air to that of the fiber bundle. The dimensionless velocity (Eq. 4) is taken as the ratio of measured liquid invading velocity to measured capillary velocity. The capillary velocity was estimated from the flow image and confirmed by Eq. 3. With this model it is possible to describe the very slow filling case in which the liquid penetration inside the fiber bundles is faster than the external liquid-invading velocity. The model prediction agrees qualitatively with the experimental results of micro voids entrapped inside the fiber bundles (see Figure 17, Part I).

Liquid penetration in regular fiber bundles and air compression

After the initial air trapping, the liquid keeps penetrating into the core of fiber bundles until the pressures inside and outside the air bubble are in equilibrium. In our visualization experiments, we observed that the real nature of liquid penetration is heterogeneous. However, in order to simplify the flow field, a homogeneous penetration model is introduced here. The model takes into account the effect on void size of the pressure difference between the inside and outside of the fiber bundle. The rate of penetration can be expressed as the following equation (Parnas and Phelan, 1991; Skartsis et al., 1992b; Chen, 1993):

$$\phi_b \frac{dr}{dt} = -\frac{K_b}{\eta} \frac{(P_m + \Delta P_{cap}) - \dfrac{P_0 r_0^2}{r^2}}{r \ln(r_0/r)}, \qquad (11)$$

where r is the radial penetration flow front inside the fiber bundle, P_m is the pressure of the fiber mats, and P_0 is ambient pressure, that is, the pressure inside the fiber bundle at initial air bubble radius r_0. Parnas and Phelan (1991) initially derived a similar equation. Here we include ΔP_{cap} in order to take into account the effect of surface tension.

For a constant flow rate system, the inlet pressure will increase with respect to time while the main flow velocity remains the same. The effect of flow into fiber bundles will be to decrease the velocity. Figure 6 illustrates this effect. The front velocity decreases about 10% at the end of the mold and the inlet pressure builds up as liquid injection continues. The dimensionless front velocity and dimensionless filling time are scaled to the initial front velocity and mold-filling time. The dimensionless pressure drop is defined as P_m/P_0.

The void size distribution across the mold after filling and the initial void size just behind the flow front are shown in Figure 7. The initial void size behind the flow front decreases a little bit due to the slight decrease of front velocity. The voids closest to the mold entrance have the smallest size since there the pressure rise is highest. The dimensionless void size is defined as the ratio of entrapped air diameter to that of the fiber bundle. Because of the initial liquid bypassing and air-trapping effect, the initial void size behind the flow front at the mold entrance is less than that of the fiber bundle.

With higher viscosity or velocity the pressure rise will be higher (Eq. 1), and the void size will decrease. The effects of porosity and vacuum on void size distribution are shown in Figures 8 and 9. Liquid velocity and viscosity are kept the same (unit viscosity and unit velocity) for these calculations. The effect on void size is again mainly due to the pressure rise. It is clear that the vacuum has the strongest effect on void size. Vacuum increases the pressure differential outside and inside the voids, thus reducing the void size tremendously. With lower porosity or higher fiber loading, the pressure increases, and therefore the void size decreases.

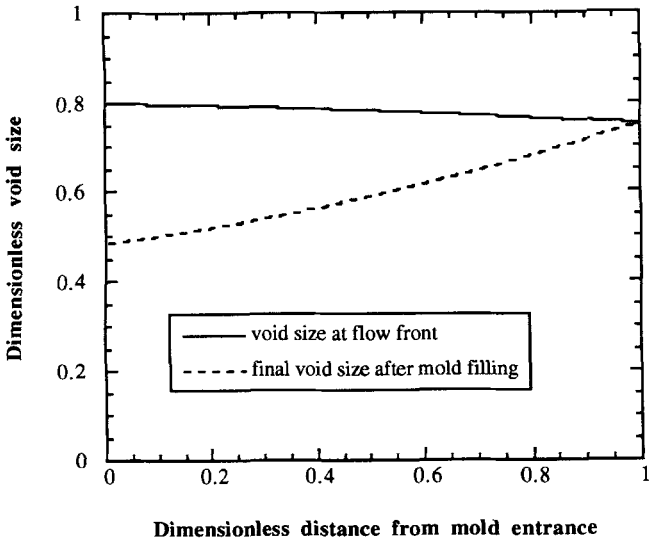

Figure 7. Void size evolution at flow front and variation after mold filling.

Dimensionless void size is the ratio of entrapped air diameter to that of fiber bundle. Initial trapping due to bypassing is included.

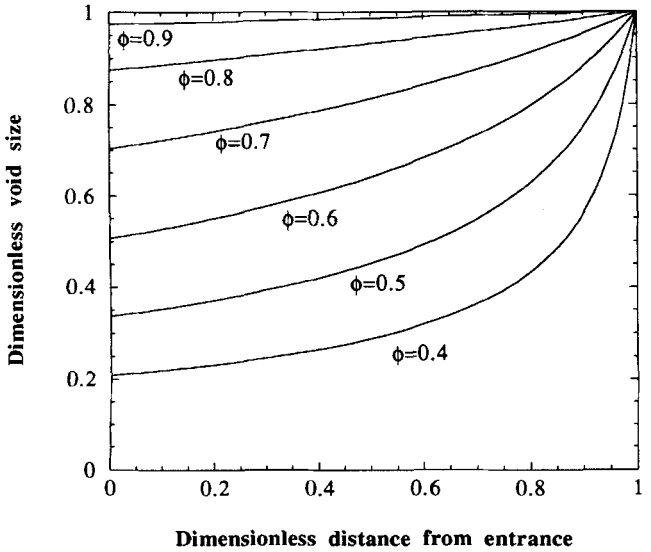

Figure 8. Effect of fiber content on void size distribution after mold filling.

Dimensionless void size is the ratio of entrapped air diameter to that of the fiber bundle. Assume fully trapped initially.

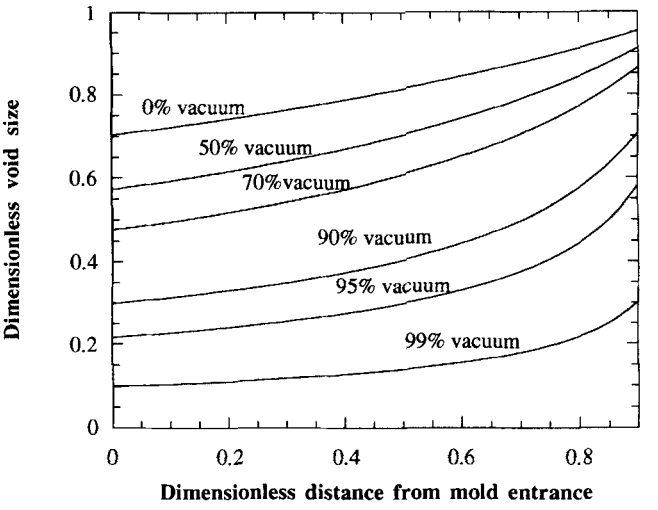

Figure 9. Effect of vacuum on void size distribution after mold filling.

Dimensionless void size is the ratio of entrapped air diameter to that of the fiber bundle. Assume fully trapping initially.

Mobilization model

The models just proposed only take into account homogeneous trapping and penetration. In reality the pore spaces between fibers are not identical. During the penetration process the entrapped air bubbles are still in a transient state. These voids, inside the fiber bundles, can be forced out of the fiber bundles when the viscous force is greater than the capillary force. This is the mobilization mechanism. The governing equations of mobilization are discussed in what follows.

The pressure required to move the gas through small capillaries or pore throats is high. Cardescu (1930) investigated the resistance to force an isolated bubble of gas into a capillary constriction. As expected from the Young–Laplace equation, he found that the pressure required obeyed the equation:

$$\Delta P_{\text{cap}} = 2\sigma\left(\frac{1}{r_t} - \frac{1}{r_b}\right), \tag{12}$$

where ΔP_{cap} is the capillary pressure drop between the forward and rear surface of the gas bubble, r_t is the radius of the constriction or throat, r_b is the radius of the gas bubble body, and s is the interfacial tension.

The pressure required to mobilize a gas bubble in the glass fiber mats is expressed as (Ng et al., 1978)

$$\Delta P = |\nabla P| L\cos\alpha = \frac{\eta v}{K_{\text{eff}}} L\cos\alpha, \tag{13}$$

where α is the angle between the fiber and incoming liquid, v is the interstitial velocity of the liquid, K_{eff} is the effective permeability of the fiber bundles, and L is length of the bubble. Taking into account the multiple pore throats, Ng et al. (1978) developed an expression for the net capillary pressure difference from an average throat constriction radius, r_t, and an average body waist radius r_b:

$$\Delta P_{\text{cap}} = \frac{2\sigma}{r_t}\beta;\ \beta = 1 - \frac{r_t}{r_b}, \tag{14}$$

where β is a geometric factor that is somewhat less than unity and depends on pore space configuration. Thus the critical condition to mobilize a void inside fiber bundles can be obtained by combining the previous two equations:

$$\text{Ca}^* = \left(\frac{\eta v}{\sigma}\right) = \left(\frac{\beta K_{\text{eff}}}{r_t r_b}\right)\left(\frac{2r_b}{L\cos\alpha}\right) \tag{15}$$

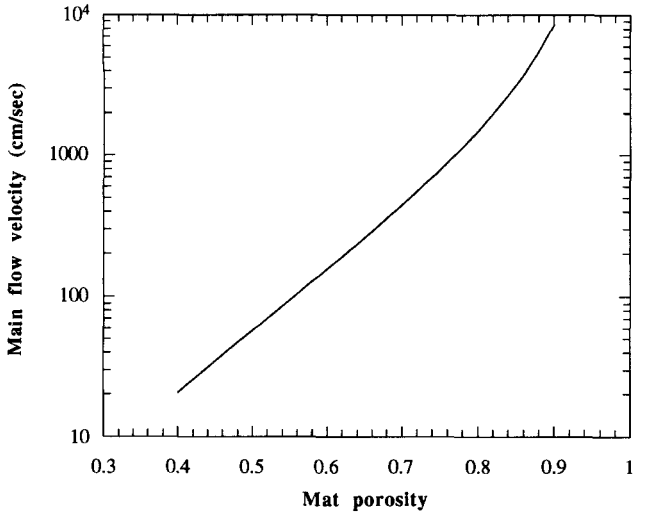

Figure 10. Critical velocity of main flow for inside bundle air bubble mobilization as a function of porosity.

Critical capillary number is taken as 2.85×10^{-3}, fluid is pure immersion oil.

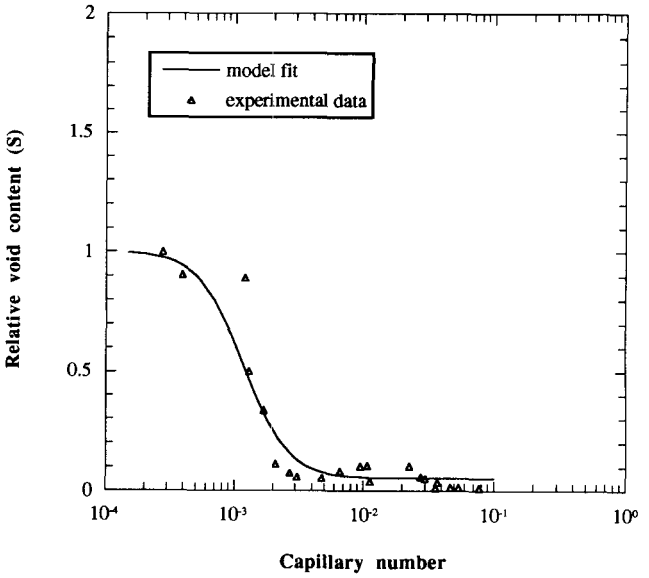

Figure 11. Void area fraction as a function of capillary number inside the fiber bundle.

Critical capillary number is approximately 1.5×10^{-3}. Test fluid is pure immersion oil. Solid line is the model prediction.

where Ca^* is the critical capillary number. At the capillary number Ca^* all bubbles of length L and longer will be mobilized. Consider, for example, a typical fiber bundle. If the fiber diameter is 15 μm, and ϕ is 0.38, the permeability will be 1.78×10^{-9} cm^2 according to Kozeny's equation (Eq. 2). Assuming that the geometric factor is 0.8, r_t equals 2 μm, $\cos(\alpha)$ is 0.5, and bubble length is 100 μm, we find the critical capillary number to be approximately equal to 2.85×10^{-3}. This number is close to the critical capillary number for reservoir oil mobilization (Melrose and Brandner, 1974; Chatzis and Morrow, 1984). With this critical capillary number and the values of the surface tension and viscosity of the immersion oil, the critical interstitial velocity inside the fiber bundle for air bubble mobilization is estimated to be 0.165 cm/s. This result can be used readily to calculate the critical interstitial velocity outside fiber bundles (mat level velocity) since the pressure gradient will be the same at both the mat level and the bundle level. The critical velocity needed to mobilize the air bubbles inside fiber bundles for the main flow vs. porosity is plotted in Figure 10. For the fiber porosity used in our experiment, $\phi = 0.75$–0.85, the required critical velocity is about 1,000 cm/s. Thus, it would be practically impossible to remove all the microvoids by mobilization from a homogeneous bundle. For the highly filled industrial application ($\phi = 0.55$–0.65) the required critical velocity is still high —about 100 cm/s. It should be pointed out that our system is limited to the surface tension range (20 ~ 40 dyne/cm), while in the case of oil recovery, the surface or interfacial tension can be as low as 10^{-3} dyne/cm.

A set of experiments was performed to test the mobilization mechanisms inside fiber bundles using large unidirectional fiber bundles. The fibers were aligned transverse to the flow direction and close packed so that there was no passage between the fibers and glass plates. The liquid was forced to pass through fiber bundles. In this case there was only one porosity level, namely the fiber bundle level. This represents the case of highly filled composites processing. The residual void content as a function of capillary number is shown in Figure 11. At higher filling rate or capillary number, the quantities of voids decreased with increasing flow rates. No meso voids occurred in this experiment due to the tight fiber network.

Of interest here is the question of how well the proposed models predict the void content during the RTM/SRIM process. As mentioned earlier, our proposed simple air-entrapment model can predict only initial air trapping and capillary invasion of regular fiber bundles/air compression. A model with capillary invasion of disordered fiber bundles in a three-dimensional network must be included in order to fully describe the true fiber-wetting process. However, we introduce an engineering approach to estimate the void content based on the current simple models. We define a mobilization efficiency factor by fitting the experimental data between void content and capillary number. Then the overall void content can be estimated from the equation:

$$\text{Void fraction} = (\text{initial void size})\times(\text{fiber volume fraction})\times\Lambda \quad (16)$$

where $\Lambda = (\text{compression factor})\times(\text{mobilization factor})$, the compression factor can be estimated by the pressure rise from the air compression model, and the mobilization efficiency, which can be experimentally determined.

From the relationship between void content and capillary number (Figure 11), one can fit the data with the following equation:

$$\frac{1-S}{S-S_\infty} = (K_3 Ca)^m, \quad (17)$$

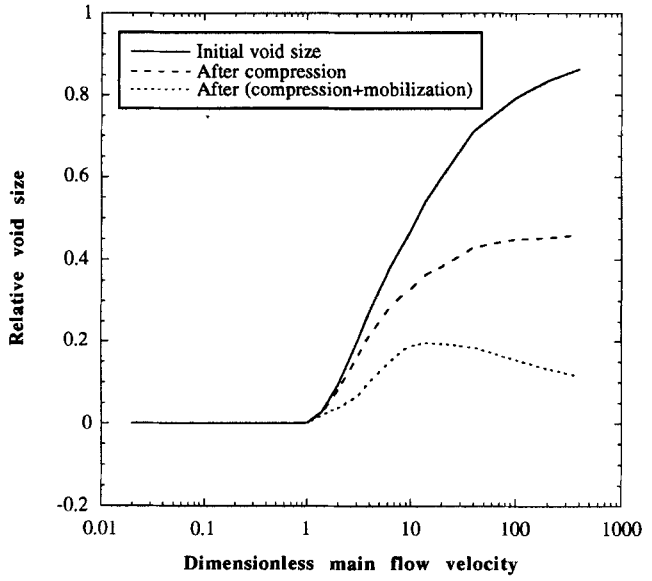

Figure 12. Relative void size after compression vs. mobilization.

where S is the relative void content (inverse of mobilization efficiency), S_∞ is the infinite or residual relative void content, K_s is some constant, Ca is the capillary number, and m is some exponent to fit the data. Figure 11 also shows the model fit to the experimental data of void contents vs. capillary numbers inside fiber bundles. The parameters are $S_\infty = 0.05$, $K_s = 2{,}100$, and $m = 1.2$.

Once the parameters of the previous equation are obtained, one can estimate the void content by Eq. 16. For example, we can compare the model prediction and the experimental data (as shown in Figure 13), which relates the void content as a function of injection velocity of flow transverse to unidirectional fibers. The mat porosity is 0.86, fluid viscosity is 51.5 cp, and initial ambient pressure is 1 atm. Figure 12 shows the relative void size as a function of the dimensionless fluid injection velocity (Eq. 4) after initial trapping, air compression, and mobilization. The relative void size after all three steps gives the final void size inside each single fiber bundle. This final void size times a fiber volume or area fraction gives the void content at a particular position. Figure 13 gives a comparison between experimental data and model prediction. The agreement is reasonable considering all the simplifications and assumptions made. The initial increase of void content in the curve is due to the increase of fluid bypassing. Then the void content reaches a maximum and gradually decreases due to the mobilization effect. Notice that the model prediction is based on the assumption that the experiments reach equilibrium. In a real RTM/SRIM process, the dynamic nature of mold filling and possible turbulent flow at high flow rates must be considered as a design parameter. One can use the same approach to predict the void content inside fiber bundles in the case of continuous random fiber mats or flow parallel to the unidirectional fibers.

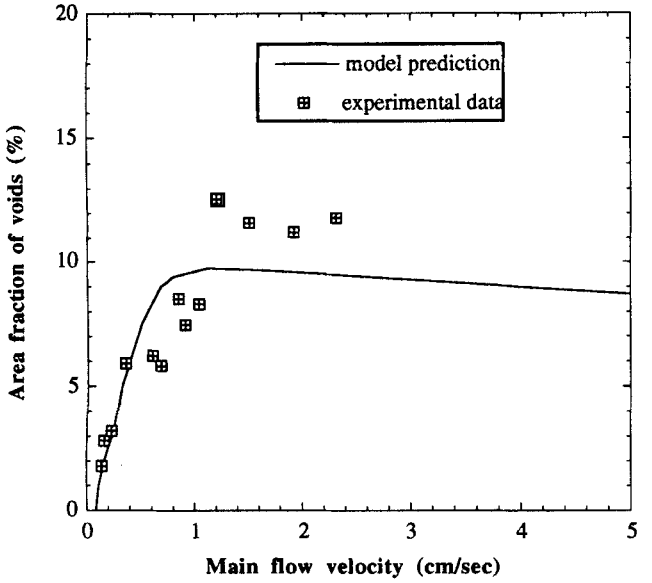

Figure 13. Model prediction vs. experimental data of void content for transverse fiber experiments (data from Figure 17 of Part I).

Conclusions

In this study we explain our experimental observations with the aid of a simple air-entrapment model that is based on the concept of two levels of porosity in fiber mats. A simple model, which includes liquid bypassing and initial air trapping, subsequent capillary invasion of regular fiber bundles and air compression, and mobilization, is proposed to explain air-entrapment phenomena during flow transverse to fiber bundles. The model successfully explains the phenomena of liquid bypassing and air trapping during the initial contact. A simple homogeneous penetration model with an ideal gas law is also successfully applied to describe the air compression behavior. An empirical mobilization efficiency equation is adapted into this model to estimate void content. Results show that this engineering void-content model can quantitatively describe the air-trapping behavior of liquid across fiber bundles.

In reality the nature of liquid penetration inside fiber bundles is irregular and three-dimensional. It is a combination of transverse and axial fiber penetration. Future work should include the heterogeneous penetration model. With this model the effect of the contact angle on air entrapment can be analyzed. The effect of interfacial properties between fibers and resins can also be investigated. A statistical approach such as percolation theory or a Monte Carlo simulation could be applied for the network–liquid invasion study. Further experiments should include the studies that can vary the wetting properties of resins by both adding different amounts and types of surfactants and also by changing the surface coatings of fibers.

Acknowledgments

The authors thank the Center of Interfacial Engineering at the University of Minnesota, Rhone-Poulenc Inc., and Moldflow Ltd. for the financial support provided for this research. We would also like to thank the Minnesota Supercomputer Institute for their generous computational grant to make this work possible.

Literature Cited

Berman, A. S., "Laminar Flow in Channels with Porous Walls," *J. Appl. Phys.*, **24**, 1232 (1953).

Cardescu, I. I., "Behavior of Gas Bubbles in Capillary Spaces," *Trans. AIME Petrol. Div.*, **86**, 351 (1930).

Chatzis, I., and N. R. Morrow, "Correlation of Capillary Number Relationships for Sandstones," *SPEJ*, **24**, 555 (Oct., 1984).

Chen, Y. T., H. T. Davis, and C. W. Macosko, "Wetting of Fiber Mats for Composites Manufacturing: I. Visualization Experiments," *AIChE J.*, **41**, (1995).

Chen, Y. T., "Resin Transfer Molding of Polycyanate: Chemorheology, Molding Experiment, and Wetting Visualization," PhD Diss., Univ. of Minnesota, Minneapolis (1993).

Gonzalez, V. M., "Studies of Reactive Polymer Processing with Fiberglass Reinforcement," PhD Diss., Univ. of Minnesota, Minneapolis (1983).

Macosko, C. W., *Fundamentals of Reaction Injection Molding*, Hanser, New York, p. 209 (1989).

Melrose, J. C., and C. F. Brandner, "Role of Capillary Forces in Determining Microscopic Displacement Efficiency for Oil Recovery by Waterflooding," *J. Can. Pet. Tech.*, **13**(4), 54 (1974).

Ng, K. M., H. T. Davis, and L. E. Scriven, "Visualization of Blob Mechanics in Flow Through Porous Media," *Chem. Eng. Sci.*, **33**, 1009 (1978).

Parnas, R. S., and F. R. Phelan, Jr., "The Effect of Heterogeneous Porous Media on Mold Filling in Resin Transfer Molding," *SAMPE Q.*, 53 (Jan. 1991).

Skartsis, L., J. L. Kardos, and B. Khomami, "Resin Flow Through Fiber Beds During Composite Manufacturing Process. Part I: Review of Newtonian Flow Through Fiber Beds," *Polym. Eng. Sci.*, **32**(4), 221 (1992a).

Skartsis, L., B. Khomami, and J. L. Kardos, "The Effect of Capillary Pressure on the Impregnation of Fibrous Media," *SAMPE J.*, **28**(5), 19 (1992b).

Van Brakel, J., and P. M. Heertjes, "Capillary Rise in Porous Media: I. A Problem," *Powder Technol.*, **16**, 75 (1977).

White, F. M., Jr., B. F. Barfield, and M. J. Goglia, "Laminar Flow in a Uniformly Porous Channel," *J. Appl. Mech.*, **25**, 613 (1958).

Manuscript received Sept. 22, 1993, and revision received Nov. 23, 1994.